Numerical investigation of the respective roles of cohesive and hydrodynamic forces in aggregate restructuring under shear flow

Akash Saxena, Jean-Sébastien Kroll-Rabotin, R. Sean Sanders

Numerical investigation of the respective roles of cohesive and hydrodynamic forces in aggregate restructuring under shear flow

Akash Saxena[a], Jean-Sébastien Kroll-Rabotin[b], R. Sean Sanders[a,*]

[a]*Department of Chemical Engineering, University of Alberta, Edmonton, AB, Canada*
[b]*Institut Jean Lamour, Université de Lorraine, CNRS, IJL, Labex DAMAS, F-54000 Nancy, France*

Abstract

Hypothesis
Aggregate structure is conditioned by a balance of cohesive forces between primary particles and hydrodynamic forces induced by the surrounding flow. Numerical simulations for different ratios between radial and tangential components of cohesive forces to hydrodynamic forces should highlight the role of the each force in aggregate restructuring under shear flow.
Experiments
Aggregates sharing similar morphological characteristics were algorithmically created. The forces between primary particles were accounted for using models taken from the literature. Aggregates with different cohesive forces were then submitted to shear by imposing a shear stress in the liquid phase. Hydrodynamic forces were calculated following two approaches: first, with a free draining approximation to extract general trends, then with immersed boundaries in a lattice Boltzmann flow solver to fully resolve the flow and particle dynamics.
Findings
Aggregate structural changes were tracked over time and their stable final size, or eventual breakage, was recorded. Their final structure was found to depend little on normal cohesive forces but is strongly impacted by tangential forces. Normal forces, however, strongly affect breakage probability. Furthermore, resistance to deformation at the aggregate scale induces a flow disturbance that reduces drag forces compared to the free-draining approximation, significantly impacting aggregate restructuring.

Keywords: Fractal aggregates, Colloidal interactions, Hydrodynamic interactions, Free-draining approximation, Lattice Boltzmann method, Discrete Element Method, Resolved hydrodynamics, Immersed Boundary Method

1. Introduction

Formation of aggregates is common in many solid-liquid processes. For example, waste water treatment often involves aggregation of particles of size range 1 to 44 μm [1] into larger units, which are easier to separate. Another example includes recovery of metallurgical inclusions (size as small as 1 μm) from liquid alloys [2]. Similarly, during pipeline transport of heavy oil, fouling due to the precipitation and aggregation of micron-sized asphaltene particles has been observed [3].

Regardless of the system, aggregate size, shape and structure are key parameters in such solid-liquid processes. Aggregate morphology determines properties such as porosity and dimensions of the solids. These properties in turn affect the solid-liquid and solid-solid interactions in the mixture, leading to changes in system rheology which directly affects the transport of the solids. While morphology of the solids affects the system properties, the flow itself can induce morphological changes to the aggregates. Particularly, shear flow can change the size and density of the particles. Therefore, the coupled response of aggregates and system properties in terms of mixture rheology and aggregate shear history has thus been studied in many fields using experimental approaches [4].

An aggregate's lifetime, from birth by collision of smaller particles (or aggregates) to its death by breakage, may last only fractions of a second [5]. Capturing phenomena with such time scales requires com-

*Corresponding author: ssanders@ualberta.ca

plex experimental setups [6–8], and even then, microscopic details such as real-time structural changes are nearly impossible to track. On the other hand, modeling and simulation of aggregates in shear flow have enabled scientists to investigate the aggregate behavior at a more fundamental level, where the physics at play can be selectively implemented to see their relative impact on aggregate behavior. Recent aggregate studies through simulations have complemented experimental results [7, 9, 10], proving the viability of numerical studies. Such numerical investigations of aggregation dynamics and aggregate restructuring have been conducted at infinitely low Reynolds conditions using Stokesian Dynamics [11], or even using the Free Draining Approximation (FDA) in which the fluid-particle interactions are simplified to consider only Stokesian drag [12].

In this study, a fully coupled Eulerian-Lagrangian approach has been developed to evaluate the restructuring of aggregates in shear flows for low but finite Reynolds numbers. In particular, a Discrete Element Method (DEM) is used for primary particle interactions and tracking as it is one of the few methods which can accommodate resolved particle-particle interactions. A lattice Boltzmann method (LBM) is used for solving the liquid flow. Both are coupled using an Immersed Boundary Method (IBM) so that any flow disturbance induced by primary particles and consequent hydrodynamic interactions are fully resolved [13]. Selected particle-particle interaction models have been implemented in the DEM to represent the mechanical behaviour of aggregates. General attractive and repulsive force models, and the bending moment as described by Pantina and Furst [14], have been included.

Artificial aggregates were created and characterized using fractal dimension and radius of gyration. The evolution of these shape indicators over time has been studied while aggregates are subjected to a shear flow. Preliminary results obtained with fully coupled liquid-solid simulations were also compared with results based on FDA. Not only does FDA provide computationally economical insights into the effect of particle-particle interactions, the results obtained through FDA also act as a point of reference to highlight the effect of hydrodynamic interactions. In fully coupled simulations, significant perturbations in the flow field were observed due to the presence of particles, which leads to significantly different aggregate structures. This provides a novel perspective into the hydrodynamics, showing that damping of the strain rate around an aggregate results in a shielding effect on particles in the periphery of the aggregate. The cohesive force between a pair of particles is described as the combination of a tangential force and a normal force. The tangential force is applied in the direction perpendicular to the line-of-centers between primary particles. It imparts a bending moment to the aggregate. Normal cohesive forces are applied in the direction of the line-of-centers. Together, combinations of normal and tangential components can be used to model short-range particle-particle interactions, making the results applicable to non-DLVO interactions. The contributions of these interactions and their underlying impact on aggregate restructuring have been compared, at a given shear rate. This is a pioneering study in establishing the respective roles of tangential and normal forces in aggregate restructuring and breakage. While increased shear produced denser aggregates, the effect of tangential forces on aggregate morphology appears to be more complex. Also, larger tangential forces were found to make aggregates brittle, that is, they were resilient to restructuring but prone to breakage.

2. Governing physics in aggregate restructuring under shear flow

Aggregate structure refers to the spatial organization, and connectivity, of the constituent primary particles. Aggregate restructuring can be defined as change in structure without breakage or fragmentation. The extent of restructuring can be quantified using morphological parameters such as fractal dimension and radius of gyration. Particles within an aggregate are held together by the cohesive forces, such that the aggregate is in a structural equilibrium. When aggregates are transported in a liquid phase, they experience hydrodynamic forces that compete with the cohesive forces holding them together. Consequently, aggregate morphology evolves according to the balance of the cohesive forces holding the aggregate together and the external hydrodynamic forces. This happens through re-distribution of the hydrodynamic stresses and the cohesive forces within the aggregate [15]. When the hydrodynamic forces are not balanced by the combined cohesive forces within an aggregate, it will restructure and/or eventually break [10].

Normal cohesive forces, such as van der Waals interactions, hold particles within an aggregate, at separation distances much smaller than the particle size. Therefore, the particles are practically bonded to each other through the cohesive forces. The relation between normal cohesive forces and aggregate restructuring and breakage has been discussed extensively in the literature. For example, Zeidan et al. [16] found that aggregates ruptured at low cohesive forces, while relatively higher cohesive forces lead to breakage through erosion

of particles. Kroupa et al. [17] observed that higher normal cohesive forces produced larger stable aggregates in similar hydrodynamic conditions. These studies clearly showed that strong cohesive forces are necessary for strong aggregates. Furthermore, Kroupa et al. [17] also showed that it is only the maximum attractive force that determines structural evolution of an aggregate. However when it comes to restructuring, normal forces have been shown to have little impact while tangential forces reduce restructuring [18].

Some studies have covered the relative effect of forces on aggregate evolution [18, 19] by approximating the hydrodynamic forces through FDA, where primary particles comprising an aggregate do not see any disturbance in the flow due to the presence of other particles. To account for the role of hydrodynamic interactions, numerical investigations of aggregate behaviour at very low Reynolds number have been conducted using Stokesian Dynamics (SD). Some of these studies focused on cohesive force distribution in rigid aggregates [20–22], and have related the hydrodynamic stresses to a stable critical size of aggregates. Other studies identified a power law relation between the hydrodynamic stresses and the critical mass of the aggregates [5, 23, 24].

Finally, studies resolving the hydrodynamics using SD and their impact on aggregation [11, 25], restructuring [10, 26, 27] and breakage kinetics [5] have shown how aggregates evolve under different hydrodynamic stresses, but are still not numerous enough to cover the full set of parameters at play. For example, Horii et al. [10] did not include the tangential forces which have been seen to be rather crucial in restructuring. Furthermore, since SD uses multipole expansion of the velocity field to solve the linear Stokes equations, it is restricted to low Reynolds number conditions. Consequently SD simulations are likely to produce inaccurate predictions of hydrodynamic interactions whenever the shear rates are high or the aggregates are too rigid to restructure, in which case inertial effects at aggregate scale appear. Overall, even with these recent studies, there is a knowledge gap in the understanding of aggregate evolution in shear flow. Firstly, the role of constituent primary particle interactions in aggregate evolution, especially on breakage, is not well documented. Secondly, while the importance of resolved hydrodynamics has been demonstrated, their effects on restructuring and breakage have not been thoroughly investigated.

3. Simulation setup and numerical methods

This paper aims to relate aggregate restructuring to the normal and tangential components of cohesive forces between its constituent particles. To do so, the usual interaction potentials for colloidal particles (such as van der Waals and Born repulsion) have been used. However, the results have been interpreted by considering only the maximum values of the force components. Therefore, the observations do not depend on the underlying interaction potential. Breakage events are recorded in order to distinguish conditions under which aggregate evolution kinetics are driven by breakage (and eventual re-aggregation) or restructuring. First, a model with simplified hydrodynamics using FDA is used. Through FDA, the role of cohesive forces between constituent particles is established. Then, a lattice Boltzmann method, where particles are represented using an Immersed Boundary Method, is used to fully couple aggregate and flow dynamics.

3.1. Modelling of the physical problem

The objective of the numerical investigations is to capture and quantify the morphological evolution of aggregates in shear conditions that are representative of transport and mixing processes. In such processes, shear is induced by wall shear stress, and by turbulent agitation. Small aggregates are typically smaller than the Kolmogorov length scale of the turbulent flows that carry them. Therefore, the flow field that drives their restructuring is approximated by a plane shear flow, which combines a strain [7, 8, 10] with a rotation. Fig. 1 shows the velocity field in a plane shear flow in the vicinity of an aggregate. The aggregate is placed at the center of the domain and is free to move and rotate according to the forces it experiences.

While aggregates undergo shear flows, process quantities such as energy dissipation are often used to estimate shear stresses in the flow. In the idealized case of a plane, the shear stress tensor is reduced to one off-diagonal component and can thus be characterized by a single value τ. In a Newtonian fluid, such as water, there is a direct relation between the shear stress and the resulting shear rate $\dot{\gamma}$:

$$\dot{\gamma} = \tau/\mu \tag{1}$$

where μ is the dynamic viscosity of the fluid. Using this relation, all following simulation data are processed with shear rate as a parameter, even when shear stresses were the actual control parameters in simulations.

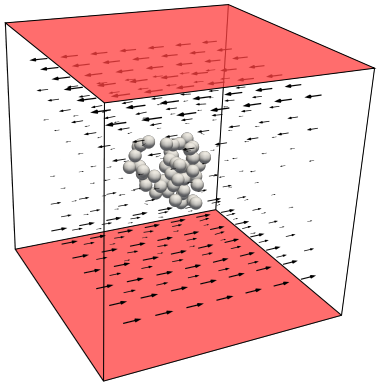

Figure 1: Domain setup for simulations with hydrodynamics. The arrows show the flow induced through top and bottom walls.

To study aggregate restructuring, aggregates were placed in simulated, simple plane shear flows. The hydrodynamic forces from the liquid phase that are endured by the aggregates were either modelled through analytical approximations or calculated by resolving the flow. For the latter part, a lattice Boltzmann method coupled with the solid phase through an Immersed Boundary Method was used. As stated earlier, aggregate restructuring depends on the balance between hydrodynamic forces and the cohesive forces between constituent primary particles.

Cohesive forces between primary particles were thus implemented and characterized by their maximum values; that is, the one that needs to be overcome by the drag force from the flow in order to break the bonds between them. Then, the morphological evolution of aggregates was recorded by tracking the variations of their radii of gyration over time. To extract average trends, all simulations were repeated for a set of 10 different aggregates comprised of the same number of particles, and the same initial radius of gyration.

With the flow characterized by its shear rate $\dot{\gamma}$ and an aggregate by its radius of gyration R_g, the aggregate Reynolds number is defined as

$$\mathrm{Re} = \frac{4\dot{\gamma}R_g^2}{\nu} \tag{2}$$

which varies over the duration of a simulation since R_g varies. In some simulations presented later, R_g can be 1.8 times greater than its initial value corresponding to a multiplication of this Reynolds number by more than 3. However, the primary particle Reynolds number Re_p is constant since R_p, the primary particle radius, is fixed, so that

$$\mathrm{Re}_p = \frac{4\dot{\gamma}R_p^2}{\nu} \tag{3}$$

3.2. Coupling aggregate dynamics and hydrodynamics

Although FDA is an approximation of the hydrodynamic action on the particles, its simplicity in implementation and low computation times makes it a valuable tool to study aggregate evolution in simple shear flows. Thus, it has been widely utilized [12, 18, 28–30]. Because FDA cannot fully capture the hydrodynamic effects on aggregate restructuring, and such interactions are known to play a significant role in the restructuring of aggregates [18, 27, 31], they have been resolved in this study using a lattice Boltzmann method (LBM).

3.2.1. Free Draining Approximation (FDA)

Aggregates are introduced to a shear profile characterized by its shear rate $\dot{\gamma}$. In FDA, the effect of the flow on each particle in an aggregate is modelled through the shear force and torque that are responsible for driving the aggregate evolution. One way to calculate this shear force ($F_{f/p}$) and torque ($T_{f/p}$) is by using Stokes' drag law as

$$\boldsymbol{F}_{f/p} = 6\pi\mu R_p(\boldsymbol{v}_p - \dot{\gamma}\, z\, \boldsymbol{e}_x) \tag{4}$$

$$\boldsymbol{T}_{f/p} = 8\pi\mu R_p^3(\boldsymbol{\omega}_p - \frac{1}{2}\,\dot{\gamma}\, \boldsymbol{e}_y) \tag{5}$$

This method assumes that the flow is not affected by the particles, so that hydrodynamic interactions between particles within an aggregate are not considered. Thus, it tends to overestimate the hydrodynamic forces as it does not compensate for the surface of a particle shielded from the flow by other surrounding particles [9, 32–35]. This phenomenon is commonly referred to as the "shielding effect". Some studies have made attempts to correct for the shielding effect either by calculating the area of the aggregate exposed to the shear flow [9], or by correcting the shear forces by comparing with hydrodynamic forces for resolved particles [18], but in the end local hydrodynamics always strongly rely on models and are only loosely approximated in FDA. Despite these drawbacks, FDA has been widely used to study aggregate evolution due to its simplicity and computational efficiency [12, 18, 19]. Since FDA overestimates the hydrodynamic forces, it can be expected that a relative study of forces will yield qualitatively the same results as a study done with fully resolved hydrodynamics. Therefore, FDA was used for an initial study of the forces involved in aggregate restructuring.

3.2.2. Fully resolved hydrodynamics

To accurately account for the hydrodynamics, a lattice Boltzmann method is coupled with a Discrete Element Method through an Immersed Boundary Method. The LBM used in this research was first published by Eggels and Somers [36] and extensively described in the more recent work of Sungkorn and Derksen [37]. It is coupled with the solid phase using the IBM presented by Niu et al. [13]. Particle diameter is discretized over 10 lattice nodes, and the domain size is set to $198 \times 198 \times 198$ lattice nodes. The details of this LBM approach and its coupling with the solid phase through IBM have been described in a previous work [31]. As discussed in Saxena et al. [31], the particles are tracked individually and the surface of each particle is discretized by Lagrangian marker points. It must be pointed out that the volume within the solid body is seen as fluid in the Eulerian representation of the flow. The momentum of this fluid enclosed in the sphere must also be accounted for in the momentum balance equations. One way to treat this is by making the enclosed fluid within each particle behave as a solid body. This is achieved with layers of Lagrangian marker points also on the inside of the sphere. The diameters of the primary spheres in aggregates span over 10 LBM meshes and their surfaces are covered by 1302 regularly distributed marker points for the IBM. The inner layers consist of 326 and 82 Lagrangian marker points at distances of 0.7 and 0.3 times the sphere radius, respectively. These points ensure that the flow inside the solid particles follows the motion of the solid body. The action on the marker points by the fluid inside the spheres is subtracted from the total IBM force to obtain the force of the surrounding fluid acting on the solid particle. Since the fluid inside the sphere behaves as a solid body, the force and torque produced by the enclosed fluid can be calculated as

$$\boldsymbol{F}^{\text{in}}_{f/p} = \rho \frac{4\pi}{3} R_p^3 \frac{\mathrm{d}\boldsymbol{v}_p}{\mathrm{d}t} \tag{6}$$

$$\boldsymbol{T}^{\text{in}}_{f/p} = \rho \frac{8\pi}{15} R_p^5 \frac{\mathrm{d}\boldsymbol{\omega}_p}{\mathrm{d}t} \tag{7}$$

which makes the physical force applied by the liquid flow on the sphere

$$\boldsymbol{F}_{f/p} = \boldsymbol{F}^{\text{IBM}}_{f/p} - \boldsymbol{F}^{\text{in}}_{f/p} \tag{8}$$

$$\boldsymbol{T}_{f/p} = \boldsymbol{T}^{\text{IBM}}_{f/p} - \boldsymbol{T}^{\text{in}}_{f/p} \tag{9}$$

where $\boldsymbol{F}^{\text{IBM}}_{f/p}$ and $\boldsymbol{T}^{\text{IBM}}_{f/p}$ are the total momentum exchange between the liquid phase and the marker distribution [13]. Such inertia corrections are included in the numerical resolution of the particle as a force and a torque that depend on particle acceleration.

To induce flow, shear stresses are imposed at the top and bottom planes of the simulation domain, illustrated as red planes in Fig. 1. To impose a controlled shear stress, the boundaries are treated as free-slip at the LBM level and an extra source term is added to the liquid layer adjacent to the free-slip boundary condition. The other boundary conditions, in streamwise and spanwise directions, are periodic. The liquid is initially at rest and the aggregate inside is not moving. When the simulation begins the fluid starts to be sheared under the combined action of stresses on the top and bottom planes.

3.3. Aggregate creation and characterization

Aggregate size and density are the most obvious quantities to characterize its structure [38]. Radius of gyration (R_g) is widely used to quantify aggregate size. In the context of aggregates, R_g^2 is defined as the ratio of the second moment of mass around the center of the aggregate to the total mass:

$$R_g^2 = \frac{1}{m} \int r^2 \mathrm{d}m \tag{10}$$

For an aggregate consisting of N primary particles, as long as their size is small compared to the aggregate size ($R_p \ll R_g$), the radius of gyration of the aggregate can be approximated as

$$R_g = \sqrt{\frac{\sum_{i=1}^{N} m_i r_i^2}{\sum_{i=1}^{N} m_i}} \tag{11}$$

where r_i is the distance between particle i and the center of gravity of the aggregate, and m_i is its mass. If primary particles have the same mass, it simplifies as

$$R_g = \sqrt{\frac{\sum_{i=1}^{N} r_i^2}{N}} \tag{12}$$

On the other hand, density is widely reported as aggregate fractal dimension D_f obtained through techniques such as light scattering [7], imaging and settling [6]. However, Gmachowski [39] showed that D_f depends only on two parameters: R_g and the number of particles N in an aggregate. Therefore, if the number of constituent particles within an aggregate remains the same (that is, the aggregate does not break), R_g can be used to represent density. Essentially, R_g reflects the distribution of mass in an aggregate relative to its center of mass: the lower its value, the more densely packed the aggregate. Another parameter sometimes used for density measurement is the ratio of hydrodynamic radius

R_h to radius of gyration. However, Harshe et al. [40] showed that R_g/R_h varies roughly between 1.0 and 1.3 as the density changes, and therefore R_g can be reasonably used to estimate R_h. When R_g is normalized by the radius of the constituent primary particle (R_p), it gives the relative size R_g^* of the aggregate as

$$R_g^* = R_g/R_p \tag{13}$$

Since all aggregates in this work have the same number of primary particles, the dimensionless radius of gyration R_g^* is a useful aggregate morphological parameter that reflects both aggregate size and density: bigger aggregates with the same number of particles are less dense.

The initial aggregates were produced algorithmically, which are shown in Fig. 2. The aggregate creation algorithm takes two parameters: the number of primary spherical particles in the aggregate, and a target radius of gyration. After the first pair of particles, all other spheres are added iteratively to the aggregate. Each new sphere position is chosen among sixteen (16) random positions on a randomly selected sphere from the already added spheres. The positions that lead to particle overlap are discarded and the new sphere is created at the remaining position that yields the radius of gyration closest to the target value. This process is repeated until the aggregate contains the desired number of primary particles.

It must be pointed out that the method of aggregate generation is expected to have little impact since the aggregates experience significant restructuring in the first rotation, and the final structure is obtained after several more rotations. Therefore, the final structure is expected to reflect the effect of the shear flow more than the method of aggregate generation.

The aggregates used in these simulations are composed of 50 primary particles. Each primary particle has a radius R_p of 1 μm, and each aggregate has a radius of gyration ratio $R_g^* = 4.55 \pm 0.02$. This latter value corresponds to a fractal dimension of 2.3, according to the empirical expression given by Gmachowski [39]. The number of primary particles is chosen so that the aggregates show a fractal structure while remaining small enough to keep the simulation time within practical limits. The fractal dimension is set to 2.3 because it is a value widely observed for colloidal aggregates [32, 41–44].

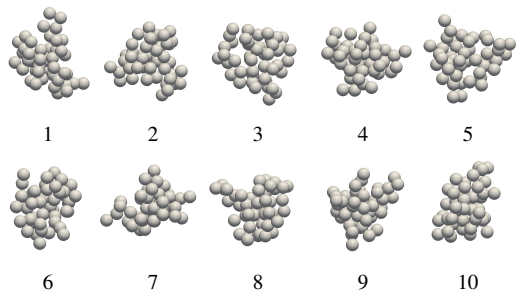

Figure 2: The 10 algorithmically created aggregates that have been used as initial conditions in the simulations ($N = 50$, $R_p = 1\,\mu\text{m}$, $R_g = 4.55\,\mu\text{m}$).

The simulations were run for ten (10) different aggregates produced using the algorithm described above to extract general trends from their average behavior. Recall that the 10 algorithmically generated aggregates are presented in Fig. 2.

3.4. Particle interactions

The non-hydrodynamic interactions between primary particles, also referred to as cohesive forces, have been modeled according to the DLVO theory [45] which is commonly used to capture particle interactions in colloidal aggregates. In this theory, forces are derived from potentials that depend on the distance between the centers of two particles. A simplified form for the van der Waals potential between two spherical particles has been used [46]:

$$V_{\text{VdW}}(s) = -\frac{A_H}{12(s-2)} \tag{14}$$

where s is the distance between particle centers divided by particle radius, so that $s = 2$ corresponds to exact particle contact. This potential yields attractive forces that must be balanced by a very short-range force to prevent particle overlapping. Born repulsion [47] fulfils this role. For two spherical particles, the Born repulsion potential is given by

$$V_{\text{Born}}(s) = \frac{A_H N_{\text{Born}}}{s}\left[\frac{s^2-14s+54}{(s-2)^7} + \frac{60-2s^2}{s^7} + \frac{s^2+14s+54}{(s+2)^7}\right] \tag{15}$$

Although Born repulsion originates from the theory of overlapping electron clouds, its application in the study of colloidal aggregates represents a repulsive force steeper than the VDW forces, and acts as a non-overlapping force. Together, the linear dependence of VDW forces and Born repulsion on the Hamaker constant allows manipulation of the maximum attractive force by a single parameter. Since these forces act on spherical particles along the line joining the two centers, they are normal to the surfaces. Hereinafter, the

resulting force derived from van der Waals and Born repulsion potentials is thus called the normal force:

$$\boldsymbol{F}_n = -\frac{1}{R_p}\frac{\mathrm{d}}{\mathrm{d}s}(V_{\mathrm{VdW}} + V_{\mathrm{Born}})\boldsymbol{n} \tag{16}$$

Normal forces form a barrier, which must be overcome by external forces in order to break the "bond" between two particles.This barrier corresponds to the maximum attractive force F_n between two particles. Consequently, aggregate restructuring is governed by the maximum attractive force [17], regardless of the force dependence on particle distance s. Force profiles for the normal force with separation distance are further detailed in the Supporting Material Section SM 1.

Tangential forces have also been considered and modeled with the expression of Becker and Briesen [29] that applies to colloidal particles. Tangential forces induce a resistance to bending in the aggregate. In this model, the tangential force $\boldsymbol{F}_t$ acting on particle i due to its close proximity with particle j and its corresponding bending moment $\boldsymbol{T}_t$ are represented as

$$\boldsymbol{F}_t = k_t\,(\boldsymbol{\xi}_{ji} - \boldsymbol{\xi}_{ij}) \tag{17}$$

$$\boldsymbol{T}_t = 2\,R_p\,k_t\,\boldsymbol{n}_{ij} \times \boldsymbol{\xi}_{ij} \tag{18}$$

where k_t is a spring stiffness and ξ_{ij} is a spring elongation corresponding to the tangential displacement vector since the bond was created (particle "contact"). The spring stops elongating after this critical elongation $d_{\max}$ (see Section SM 2 for further details). Thus, the maximum tangential force F_t is

$$F_t = k_t\,d_{\max} \tag{19}$$

This combination of VDW, Born repulsion and tangential forces to model particle-particle interactions has produced results that compare well with experimental results [7, 29] and is therefore often found in investigations of colloidal aggregates [18, 19, 48]. Since the range of these cohesive forces is very short compared to the size of primary particles, they behave as apparent contact forces at particle scale, which is the relevant length scale for hydrodynamics and aggregate restructuring. These apparent contact forces are bounded by the maximum value of the normal and tangential force profiles, and these maxima characterize bond strength between particles in aggregate restructuring.

3.5. Particle motion

Although only the maxima of force components matter in the end, the resolution of particle motion uses smooth potentials so that the balance between hydrodynamic actions on particles and cohesive forces is achieved by letting particles adjust their distances from each other. Particle motion is thus tracked and updated by solving Newton's equation of motion for every particle following the Discrete Element Method (DEM). The equations are detailed for linear moment only, because angular momentum is solved in the exact same way, i.e.

$$m\frac{\mathrm{d}\boldsymbol{v}}{\mathrm{d}t} = \boldsymbol{F}_{f/p} + \boldsymbol{F}_n + \boldsymbol{F}_t \tag{20}$$

Equation (20) is solved for particle velocity $\boldsymbol{v}$. Due to high sensitivity of the particle-particle interactions to separation distance, a time step of 4×10^{-9}s is used. Trajectory is integrated using a first-order scheme. Details are presented in the Supporting Material Section SM 3.

In LBM+IBM simulations, the inertia of the liquid inside the particles is approximated as in Equation (6) and moved to the left hand side of Equation (20). Particle acceleration is thus calculated from Equation (20) and velocity and position are obtained through the same first-order integration scheme as used in FDA. The inertia correction from Equation (6) is only numerically stable if particle density is sufficiently greater than liquid density. Thus, particle density is taken to be twice the liquid density in the simulations. Although this value was somewhat arbitrarily chosen, the actual particle density is not important, since the Reynolds numbers remain very low and gravity force is neglected, and thus particle inertia has no impact on their dynamics. Quantitatively, the inertial effects of a primary particle can be estimated by the Stokes number, which is given in such conditions as

$$\mathrm{St}_p = \frac{1}{18}\mathrm{Re}_p \ll 1 \tag{21}$$

The results obtained with $\rho_p = 2\rho$ will thus be applicable to aggregates made of any materials, such as clay or latex, as long as they undergo low Reynolds number flow dynamics.

3.6. Tracking of aggregate evolution

Under the effect of the hydrodynamic forces from the shear flow, aggregates rotate. With rotation, the positions of particles change and so do the hydrodynamic forces acting on them. Consequently, aggregates change their structure to redistribute normal and tangential forces F_n and F_t and balance the shear they undergo. The amount of restructuring required to balance the external drag force depends on F_n and F_t. If shear forces cannot be balanced by restructuring, aggregates eventually break. In other words, the force configuration

Table 1: Simulation parameters: values of the physical constants and corresponding maximum forces.

Normal force		**Tangential force**		**Drag force**	
A_H (J)	F_n (N)	k_t (N/m)	F_t (N)	$\dot{\gamma}$ (s^{-1})	$F_{f/p}$ (N)
5.92×10^{-21}	10^{-9}	2.5×10^{-2}	10^{-9}	2.653×10^{3}	10^{-10}
5.92×10^{-22}	10^{-10}	2.5×10^{-3}	10^{-10}	2.653×10^{2}	10^{-11}
5.92×10^{-23}	10^{-11}	2.5×10^{-4}	10^{-11}	2.653×10^{1}	10^{-12}
		2.5×10^{-5}	10^{-12}		

within aggregates can lead to drastically different aggregate evolutions.

To capture the impact of different force configurations on aggregate evolution, various ratios of the normal and tangential cohesive forces to hydrodynamic forces were considered over several orders of magnitudes, and their impact on restructuring and breakage was analyzed. For any two given particles, Eq. (14) and (15) show that the maximum normal force F_n depends on the Hamaker constant A_H, which is generally of the order 10^{-20} J. Pantina and Furst [14] suggested that the resulting maximum tangential force is of the order 10^{-11} N for colloidal particles. Also, it is common to see shear rates of order 10^2 s^{-1} in experiments involving colloidal aggregates. The maximum hydrodynamic force can be estimated by the Stokesian drag relation

$$F_{f/p} \sim 12\,\pi\,\mu\,\dot{\gamma}\,R_p^2 \tag{22}$$

These simulation parameters give a base case for the maximum forces. Table 1 lists all the parameters used for controlling the forces, along with the resulting maximum force values. Each simulation case was defined by a combination of these forces, covering several orders of magnitudes for the forces considered. This allows for comparison of conditions where the components of the short-range forces are widely different. Due to the range of shear rates considered, the Stokes and Reynolds numbers at particle scale range from 10^{-4} to 10^{-2} and thus remain much smaller than 1. Consequently the inertial effects in particle motion and in the flow are negligible, so that only the ratio between the cohesive and hydrodynamic forces plays a role, not their absolute values. The normal force F_n and tangential force F_t are thus normalized by the drag force to quantify their relative effects on aggregate evolution. As a result, the dimensionless force ratios F_t^* and F_n^* vary over several order of magnitudes

$$\begin{aligned} F_n^* &= \frac{F_n}{F_{f/p}} \in \{10^1, 10^2, 10^3\} \\ F_t^* &= \frac{F_t}{F_{f/p}} \in \{10^{-2}, \ldots, 10^3\} \end{aligned} \tag{23}$$

To capture the evolution of aggregates, their dimensionless radii of gyration R_g^* were recorded over the simulation run. Fig. 3 shows the evolution tracking of Aggregate #3 presented in Fig. 2 for different values of F_n^*. Due to shear flow, the aggregate rotates and restructures. The rotation is observed only around the vorticity axis. As it restructures, its radius of gyration R_g^* fluctuates over time, and it evolves towards a denser structure. Some force ratios lead to breakage, as illustrated by the interrupted R_g^* trajectories and the cross marker in Fig. 3 for $F_n^* = 10$. Otherwise, the final size of non-breaking aggregates is quantified by their average radius of gyration over the last rotation period given by $4\pi\ \dot{\gamma}t$. Final sizes and breakage events (if any) are recorded for each of the ten (10) aggregates of Fig. 2 and for each different force configuration. The final values of R_g^* are then averaged over the surviving aggregates to give $\langle R_g^* \rangle$ which represents the average final size of the aggregate for each force ratio. This $\langle R_g^* \rangle$ is then analyzed to quantify the impact of the different forces on restructuring. The evolution of all ten aggregates for various force ratios is provided as Supporting Material Section SM 4 and Section SM 5.

All simulations were run for a period of $84.8\ \dot{\gamma}t$. Since

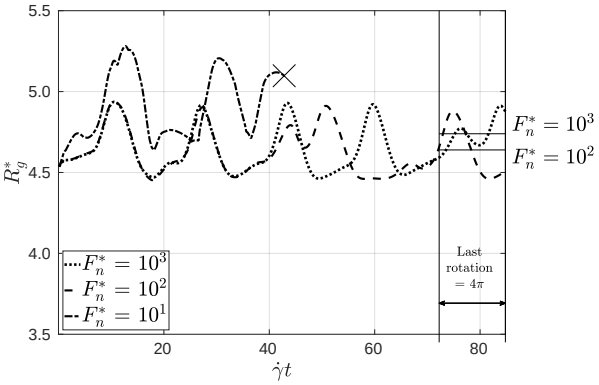

Figure 3: Illustration of aggregate evolution tracking. Breakage is marked by '×'. If an aggregate survives, its final size is taken as the average value over its last rotation period.

the fluid has a rotation rate of $4\pi\ \dot{\gamma}t$ in simple shear flow conditions, and fractal aggregates rotate at a rate close to that of a sphere, 84.8 $\dot{\gamma}t$ provides sufficient time for approximately 7 rotations for an aggregate. In each rotation, the aggregate goes through 2 cycles of compression and elongation.

4. Results and discussion

Although individual aggregate dynamic was found to be chaotic (Supporting Material Section SM 4), general trends for size are extracted for each force ratio. The radius of gyration towards the end of the evolution is averaged over all aggregates that are not broken after 84.8 $\dot{\gamma}t$. This results in one scalar value $\langle R_g^* \rangle$ that characterizes aggregate morphologies for each set of force ratios. For the aggregates that broke, the impact of forces on breakage is quantified through a "breakage probability". In this study, it is defined as the total number of aggregates broken after 84.8 $\dot{\gamma}t$ divided by the total number of aggregates, that is 10, as simulations were repeated for the 10 different aggregates presented in Fig. 2.

Eventually, the effects of the ratios of the normal and tangential forces to hydrodynamic force are quantified by comparing these two scalar characteristic values, that is the average dimensionless radius of gyration $\langle R_g^* \rangle$ and breakage probability, for various force conditions.

4.1. Effect of normal force

Fig. 4 shows aggregate evolution for various values of the normal cohesive force. Fig. 4a shows the effect of normal forces on the final structure of the aggregates that did not break. The horizontal axis is the dimensionless normal force F_n^*. The vertical axis shows the final average value $\langle R_g^* \rangle$ attained by the aggregate after evolving for 84.8 $\dot{\gamma}t$. In Fig. 4a, cases with the same tangential force to drag ratio are joined by lines. The $\langle R_g^* \rangle$ varies at most by 2.6 % even though the normal forces vary by two orders of magnitude. The small variation shows that the lines are essentially flat, indicating no impact of the normal forces on restructuring, which confirms the findings of Becker et al. [18].

Fig. 4b shows the impact of F_n^* on breakage probability: as the normal force increases, the probability that the aggregate will break decreases. As expected, when the normal cohesive force is too low, all aggregates break.

In conclusion, although the normal forces do not affect the restructuring of aggregates, they govern breakage: as long as the normal forces are strong enough to overcome the drag, they hold particles together within an aggregate; beyond that, their magnitude has no effect on the final structure of aggregates. This is consistent with the suggestion by Eggersdorfer et al. [12] that restructuring mostly occurs due to sliding of particles over each other.

4.2. Effect of tangential force

Tangential motion of particles relative to one another (sliding) depends on tangential cohesive forces. To study the effect of tangential forces, the same comparison between simulation outcomes is made for normalized tangential forces F_t^* in Fig. 5, as was done for normal forces in Fig. 4.

Fig. 5a shows the effect of tangential forces on the final structure of the aggregates. Although there is no monotonic trend, it is clear that this force plays a significant role in restructuring since $\langle R_g^* \rangle$ varies significantly when other parameters are kept constant (along the lines in Fig. 5a). Several observations can be made from inspection of Fig. 5a. First, at very high values of F_t^* (>10), aggregates do not restructure much; hence any F_t^* >10 yields values of $\langle R_g^* \rangle$ that are similar to those of the initial aggregates, that is around 4.5. On the other hand, when F_t^* <10, aggregates evolve to become denser, and their radius of gyration decreases.

Breakage probability also varies non-monotonically with tangential force as can be seen in Fig. 5b. Breakage probability reaches high values for both high and low values of F_t^*, and goes through a minimum for moderate tangential forces of $F_t^* \approx 1$. Together, Figures 5a and 5b suggest that tangential forces play a dual role in aggregate evolution. Since tangential forces induce a bending moment, high tangential forces relative to hydrodynamic actions make aggregates brittle, as they are not flexible and do not restructure to redistribute hydrodynamic stresses among bonds between constituent particles. On the other hand, tangential forces also contribute to the overall bond strength. As long as they do not prevent aggregate restructuring, increasing tangential forces makes aggregate less likely to break, which is the trend that can be seen for relatively low tangential forces. This is reflected by the non-monotonic trend seen in Fig. 5a and 5b. As the tangential forces increase beyond $F_t^* = 1$, less restructuring and more breakage are observed, showing that the aggregates become brittle with increasing tangential forces. At $F_t^* = 10^{-2}$, more restructuring and higher breakage probability are seen, indicating that there was some contribution of tangential forces to the overall bond strength.

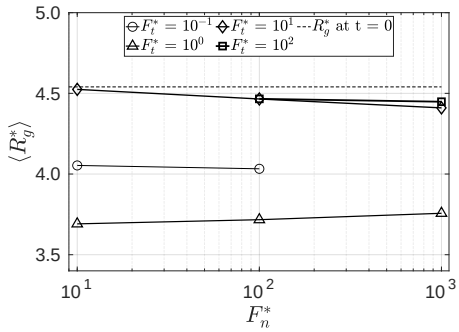

(a) Impact of normal cohesive force on radius of gyration

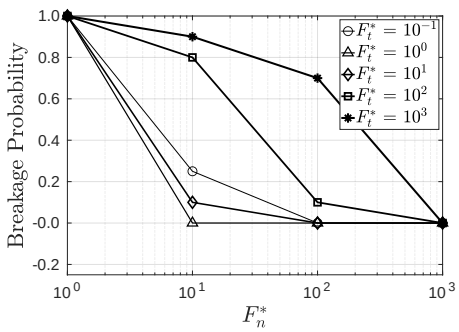

(b) Impact of normal cohesive force on breakage probability

Figure 4: Effect of normal cohesive force to drag force ratio F_n^* on (a) restructuring, (b) breakage rate.

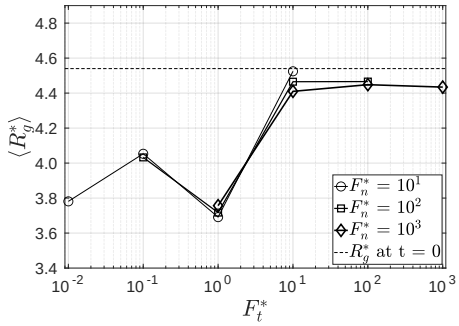

(a) Impact of tangential cohesive force on radius of gyration

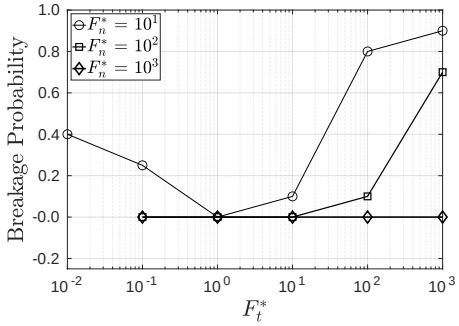

(b) Impact of tangential cohesive force on breakage probability

Figure 5: Effect of tangential cohesive force to drag force ratio F_t^* on (a) restructuring, (b) breakage rate.

4.3. Impact of hydrodynamics on aggregate restructuring

Since shear forces calculated through FDA are modelled though analytical drag laws, FDA can overestimate the magnitude of hydrodynamic forces. To quantify the impact of hydrodynamics on aggregate restructuring, the flow must be resolved. Therefore, LBM and IBM were used to accurately account for the hydrodynamics. Flow is induced by imposing a shear stress at the top and bottom planes, as shown in Fig. 1. As tangential force has been shown to play a prevalent role in restructuring, simulations cover the following conditions

$$\begin{aligned} F_{f/p} &= 10^{-10}\text{N} \\ F_n^* &= 10 \\ F_t^* &\in \{10^{-2}, 10^{-1}, 10^{0}, 10^{1}\} \end{aligned}$$

Time evolution of R_g^* shows less restructuring, especially in the first rotation, compared to the evolutions obtained through FDA for the same conditions. This is especially noteworthy during the first rotation when the algorithmically created aggregates first adjust to the flow. When the hydrodynamics are accurately resolved, less aggregate restructuring is observed, and the aggregates also break much less frequently. While small tangential forces lead to frequent breakage with FDA, this result was not observed with resolved hydrodynamics. The combination of two phenomena induced by hydrodynamic interactions between particles in the aggregate, lubrication and decrease in strain rate, are responsible for this difference in behavior. Each effect is discussed in detail in the subsequent sections.

4.3.1. Impact of lubrication on breakage

When particles move towards one another they displace the liquid between them. This displacement of liquid exerts a reaction force on the particles moving towards each other. This is known as a lubrication force. This short-range hydrodynamic force always acts against the relative motion of the particles. Due to its "stopping" nature, it acts as a repulsive force for any two approaching particles. Therefore, it effectively reduces the bond strength of the approaching particles. On the contrary, when particles close to one another tend to separate, or slide, the same motion retarding lubrication

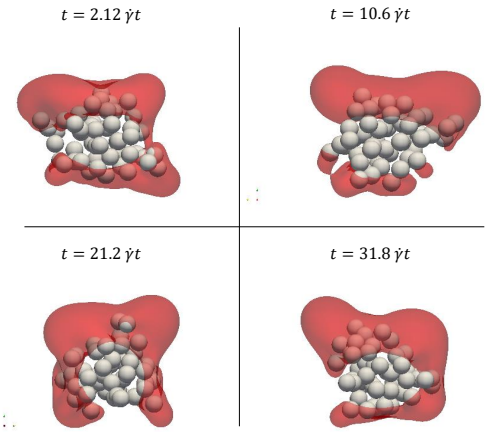

(a) Region of significant disturbance in the shear flow due to the presence of the aggregate: surface where $\|\boldsymbol{v} - \dot{\gamma}z\boldsymbol{e}_x\| = 2\,\dot{\gamma}\,R_p$

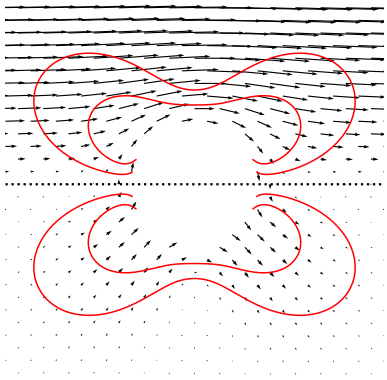

(b) Analytical solutions for the flow (top) and disturbance (bottom) velocity fields around a solid sphere in a shear flow with iso-contours of the disturbance magnitude (in red).

Figure 6: (a) Region of the shear flow that sees a significant disturbance due to the presence of the aggregate and (b) comparison with a free-to-rotate solid sphere.

force contributes to the bond strength in both tangential and normal directions. Such short-range hydrodynamic interactions increase the required force to be overcome for particles in close proximity to be separated. Therefore, these lubrication effects can explain why aggregates do not break when hydrodynamics are resolved while they would break when simulated using FDA.

The role of bond strength on breakage and restructuring was discussed earlier: bond strength has a clear impact on breakage, but its impact on restructuring is not as straightforward since tangential cohesive forces may either favor or hinder restructuring. When considering the aggregate evolution with resolved hydrodynamics (as in Fig. SM 5.1 of the Supporting Material), the cyclic amplitude of the variations of the radius of gyration R_g^* is of the same order of magnitude in all cases. However, aggregate evolution over a few rotations shows different trends: the lower the tangential force ratio, the denser the aggregates. Since short-range hydrodynamic interactions are practically the same for each case of the tangential force ratio in Fig. SM 5.1, the explanation for difference in aggregate evolution flow must come from hydrodynamic interactions at aggregate scale.

4.3.2. Disturbance of the strain rate field

It is clear that when hydrodynamics are taken into account, the whole flow is affected by the presence of the particles. Disturbances in the flow induced by the aggregate are visualized in Fig. 6. These disturbances are estimated by calculating the difference between the actual flow velocity and the analytical solution of the shear flow without solids: $\|\boldsymbol{v} - \dot{\gamma}z\boldsymbol{e}_x\|$. Fig. 6a shows in red the iso-surface where this difference is $2\dot{\gamma}R_p$ around an aggregate at different times while several iso-contour lines are plotted around a solid sphere for comparison in Fig. 6b. They show the same zones of maximum disturbance along the principal axes of strain, which are at a 45° angle. The similar features between the simulated results and the analytical solution around a solid sphere are evidence that the prevailing effect of the aggregate on the flow is to oppose the strain rate because of its own resistance to deformation. Even though colloidal aggregates do restructure, the non-deformation of the primary particles they are made of and the cohesive forces between them makes their impact on the flow close to the one of an equivalent rigid sphere, which rotates at about the same rotation rate as the rotational component of the velocity gradient, but opposes its strain component. The figures also show that maximum disturbance occurs at the periphery of the aggregate and outside of the aggregate. In its core, the flow is much less disturbed, indicating that the velocity field there is close to that of a plane shear flow. In other words, the particles in the center experience hydrodynamic forces closer to the values estimated using the Stokesian drag expression than particles at a greater distance from the center, which is in accordance with the findings of Vanni [49]. Since the Reynolds number is low, primary particles are small compared to the region of the flow governed by the viscous diffusion of momentum at the aggregate scale, which suggests that aggregate scale dynamics prevail compared to hydrodynamic interactions

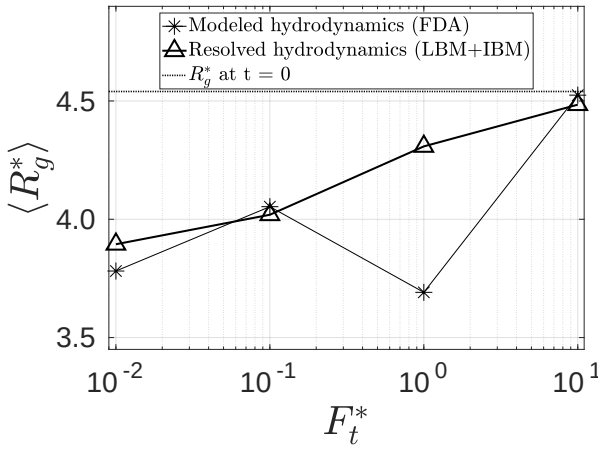

Figure 7: Impact of hydrodynamic interaction on evolution of radius of gyration with tangential cohesive force.

between pairs of primary particles.

Now, when comparing simulation results, it should be expected that differences in aggregate evolution between FDA and LBM+IBM arise in the zones of maximum disturbance. Hence, this is the modification of the flow at aggregate scale that governs restructuring rather than lubrication interactions between primary particles. Consequently, this establishes that inaccuracy of FDA does not arise due to the absence of a "shielding effect" of particles from their surrounding neighbors. Instead, the hydrodynamics are overestimated as FDA does not take into account the damping of the strain rate in the flow in the region near the periphery of aggregates. During aggregate rotation, as particles in the periphery cross the eigendirections of strain rate, they are torn apart or pushed towards the aggregate core. However, due to the resistance to deformation of the whole aggregate, including the core particles, the strain rate outside the aggregate is dampened. This disturbance is the most significant in the aggregate periphery. This results in the aggregate going through much lower strain rate variations during a rotation. The driving forces to restructuring and breakage are thus considerably decreased so aggregates restructure more slowly, and break less. However, when looking at the final structure of aggregates after $80\,\dot{\gamma}t$ (6–7 rotations) in the flow, they tend to be denser in the same way as aggregates simulated without hydrodynamic interactions do, as highlighted in Fig. 7. In other words, long range hydrodynamic interactions between particles have a strong impact on breakage rate and restructuring kinetics but have much less impact on final aggregate structure.

The comparison between modelled and resolved hydrodynamics presented in Fig. 7 sheds light on the overall impacts of hydrodynamic interactions on restructuring. By damping the strain rate field around the aggregate, hydrodynamics allow aggregates to restructure more progressively, making their evolution less dependent on how much they need to adjust to the shear flow, which is particularly significant for algorithmically created aggregates that undergo substantial restructuring. As a consequence, the relation between final aggregate structure and tangential force is smoother, and even becomes monotonic. That is also partially due to the hydrodynamic interactions contributing to apparent cohesive forces between particles as already discussed when the effects of lubrication were considered, so that actual cohesive forces have a lower relative weight in the overall dynamics. In the end, resolved hydrodynamics make aggregates less sensitive to tangential force variations. The impact of tangential cohesive forces quantitatively changes but, qualitatively it remains the governing parameter on aggregate restructuring. As shown in Fig. 7, there is a strong correlation between these two quantities, which is even more clear with resolved hydrodynamics.

Aggregate restructuring during the first rotation is less pronounced and overall aggregates are much less prone to breakage with hydrodynamic interactions. Restructuring, being more progressive, also makes aggregate fates less dependent on their initial state and as a result, all 10 aggregates show a more consistent behaviour than they did when FDA was used to approximate the hydrodynamics.

5. Conclusion

Numerical investigations of aggregate restructuring and breakage were conducted for a set of artificially created aggregates sharing the same morphological signature, in terms of radius of gyration or fractal dimension. The relative impact of the normal and tangential components of cohesive forces between aggregates on final aggregate structure and breakage probability was initially quantified using simulations that ignored hydrodynamic interactions between particles. These simulations also provided the base cases against which the role played by resolved flow hydrodynamics could be compared.

These investigations show that normal cohesive forces have no impact on restructuring, but contribute to the strength of the aggregate. On the other hand, the impact of tangential forces is more complex. Large tangential forces make aggregates brittle, making them less prone to restructuring, but more susceptible to breakage. Small tangential forces make flexible bonds in the

aggregate and decrease the bending moment of particle rods which provides greater ability to respond to the applied shear by restructuring; however, they can also make aggregates more likely to break due to weakened tangential bond strength.

The hydrodynamics at play at low aggregate Reynolds numbers include lubrication between particles, and more importantly resistance to deformation that decreases the strain rate in the flow in the periphery of an aggregate. This disturbance of the flow is thus the reason for reduced hydrodynamic driving forces on restructuring and breakage. This means that improved FDA models to account for "shielding effect" must primarily focus on the impact of the aggregate's presence on the overall shear flow [34, 50, 51] rather than of hydrodynamic models to correct interactions between primary particles [9, 52].

Complex dynamics arise in particle interactions at finite Reynolds number, even at values down to Re $\sim 10^{-2}$ [53, 54], that may have a significant impact on aggregate behaviour. The LBM as used in this research is well suited for finite Reynolds simulations, unlike SD. Work is in progress to investigate the impact of nonlinear flow dynamics on aggregate behaviour, even at low Reynolds numbers.

Acknowledgements

High Performance Computing resources were provided by Westgrid (www.westgrid.ca), Compute Canada (www.computecanada.ca), as well as by the EXPLOR centre hosted by the Université de Lorraine. The authors would like to acknowledge the financial support of the NSERC Industrial Research Chair in Pipeline Transport Processes.

References

[1] J. Masliyah, Z. J. Zhou, Z. Xu, J. Czarnecki, H. Hamza, Understanding water-based bitumen extraction from Athabasca oil sands, The Canadian Journal of Chemical Engineering 82 (2004) 628–654. doi:10.1002/cjce.5450820403.

[2] I. L. A. Daoud, N. Rimbert, A. Jardy, B. Oesterlé, S. Hans, J.-P. Bellot, 3D modeling of the aggregation of oxide inclusions in a liquid steel ladle: Two numerical approaches, Advanced Engineering Materials 13 (2011) 543–549. doi:10.1002/adem.201000355.

[3] K. Rastegari, W. Y. Svrcek, H. W. Yarranton, Kinetics of asphaltene flocculation, Industrial & Engineering Chemistry Research 43 (2004) 6861–6870. doi:10.1021/IE049594V.

[4] C. Coufort, D. Bouyer, A. Liné, Flocculation related to local hydrodynamics in a Taylor-Couette reactor and in a jar, Chemical Engineering Science 60 (2005) 2179–2192. doi:10.1016/j.ces.2004.10.038.

[5] Y. M. Harshe, M. Lattuada, Breakage rate of colloidal aggregates in shear flow through Stokesian dynamics, Langmuir 28 (2012) 283–292. doi:10.1021/la2038476.

[6] F. Vaezi, R. S. Sanders, J. H. Masliyah, Flocculation kinetics and aggregate structure of kaolinite mixtures in laminar tube flow, Journal of Colloid and Interface Science 355 (2011) 96–105.

[7] Y. M. Harshe, M. Lattuada, M. Soos, Experimental and modeling study of breakage and restructuring of open and dense colloidal aggregates, Langmuir 27 (2011) 5739–5752. doi:10.1021/la1046589.

[8] S. Blaser, Flocs in shear and strain flows, Journal of Colloid and Interface Science 225 (2000) 273–284.

[9] K. Higashitani, K. Iimura, H. Sanda, Simulation of deformation and breakup of large aggregates in flows of viscous fluids, Chemical Engineering Science 56 (2001) 2927–2938.

[10] K. Horii, R. Yamada, S. Harada, Strength deterioration of non-fractal particle aggregates in simple shear flow, Langmuir 31 (2015) 7909–7918.

[11] G. Frungieri, M. Vanni, Dynamics of a shear-induced aggregation process by a combined Monte Carlo-Stokesian Dynamics approach, in: Proceedings of the 9th International Conference on Multiphase Flow, 2016.

[12] M. L. Eggersdorfer, D. Kadau, H. J. Herrmann, S. E. Pratsinis, Fragmentation and restructuring of soft-agglomerates under shear, Journal of Colloid and Interface Science 342 (2010) 261–268. doi:10.1016/j.jcis.2009.10.062.

[13] X. D. Niu, C. Shu, Y. T. Chew, Y. Peng, A momentum exchange-based immersed boundary-lattice Boltzmann method for simulating incompressible viscous flows, Physics Letters A 354 (2006) 173–182. doi:10.1016/j.physleta.2006.01.060.

[14] J. P. Pantina, E. M. Furst, Elasticity and critical bending moment of model colloidal aggregates, Physical Review Letters 94 (2005) 138301. doi:10.1103/PhysRevLett.94.138301.

[15] U. T. Lieu, S. Harada, Stability of restructured non-fractal aggregates in simple shear flow, Advanced Powder Technology 26 (2015) 705–710.

[16] M. Zeidan, B. H. Xu, X. Jia, R. A. Williams, Simulation of Aggregate Deformation and Breakup in Simple Shear Flows Using a Combined Continuum and Discrete Model, Chemical Engineering Research and Design 85 (2007) 1645–1654. doi:10.1016/S0263-8762(07)73208-2.

[17] M. Kroupa, M. Vonka, M. Soos, J. Kosek, Size and Structure of Clusters Formed by Shear Induced Coagulation: Modeling by Discrete Element Method, Langmuir 31 (2015) 7727–7737. doi:10.1021/acs.langmuir.5b01046.

[18] V. Becker, E. Schlauch, M. Behr, H. Briesen, Restructuring of colloidal aggregates in shear flows and limitations of the free-draining approximation, Journal of Colloid and Interface Science 339 (2009) 362–372. doi:10.1016/j.jcis.2009.07.022.

[19] V. Becker, H. Briesen, A master curve for the onset of shear induced restructuring of fractal colloidal aggregates, Journal of Colloid and Interface Science 346 (2010) 32–36. doi:10.1016/j.jcis.2010.02.015.

[20] M. Vanni, A. Gastaldi, Hydrodynamic forces and critical stresses in low-density aggregates under shear flow, Langmuir 27 (2011) 12822–12833. doi:10.1021/la2024549.

[21] R. Seto, R. Botet, H. Briesen, Hydrodynamic stress on small colloidal aggregates in shear flow using Stokesian dynamics, Physical Review E 84 (2011) 041405. doi:10.1103/PhysRevE.84.041405.

[22] R. Seto, R. Botet, H. Briesen, Viscosity of rigid and breakable aggregate suspensions Stokesian Dynamics for rigid aggregates, in: Progress in Colloidal and Polymer Science, volume 139, 2012, pp. 85–90. doi:10.1007/978-3-642-28974-3_15.

[23] S. Harada, R. Tanaka, H. Nogami, M. Sawada, Dependence of fragmentation behavior of colloidal aggregates on their fractal structure, Journal of Colloid and Interface Science 301 (2006) 123–129.

[24] A. Zaccone, M. Soos, M. Lattuada, H. Wu, M. U. Bäbler, M. Morbidelli, Breakup of dense colloidal aggregates under hydrodynamic stresses, Physical Review E 79 (2009) 061401. doi:10.1103/PhysRevE.79.061401.

[25] G. Frungieri, M. Vanni, Shear-induced aggregation of colloidal particles: A comparison between two different approaches to the modelling of colloidal interactions, The Canadian Journal of Chemical Engineering 95 (2017) 1768–1780. doi:10.1002/cjce.22843.

[26] S. Harada, R. Tanaka, H. Nogami, M. Sawada, K. Asakura, Structural change in non-fractal particle clusters under fluid stress, Colloids and Surfaces A: Physicochemical and Engineering Aspects 302 (2007) 396–402.

[27] R. Seto, R. Botet, G. K. Auernhammer, H. Briesen, Restructuring of colloidal aggregates in shear flow, The European Physical Journal E 35 (2012) 128. doi:10.1140/epje/i2012-12128-4.

[28] D. Chen, M. Doi, Simulation of aggregating colloids in shear flow. II, The Journal of Chemical Physics 91 (1989) 2656–2663. doi:10.1063/1.456975.

[29] V. Becker, H. Briesen, Tangential-force model for interactions between bonded colloidal particles, Physical Review E 78 (2008) 061404. doi:10.1103/PhysRevE.78.061404.

[30] D. Liu, Z. Wang, X. Chen, M. Liu, Simulation of agglomerate breakage and restructuring in shear flows: Coupled effects of shear gradient, surface energy and initial structure, Powder Technology 336 (2018) 102–111. doi:10.1016/j.powtec.2018.05.051.

[31] A. Saxena, J.-S. Kroll-Rabotin, R. S. Sanders, A Numerical Approach To Model Aggregate Restructuring in Shear Flow using DEM in Lattice-Boltzmann Simulations, in: Progress in Applied CFD - CFD 2017, SINTEF, Trondheim, Norway, 2017, pp. 761–772.

[32] R. C. Sonntag, W. B. Russel, Structure and breakup of flocs subjected to fluid stresses: I. Shear experiments, Journal of Colloid and Interface Science 113 (1986) 399–413.

[33] R. C. Sonntag, W. B. Russel, Structure and breakup of flocs subjected to fluid stresses, Journal of Colloid and Interface Science 115 (1987) 390–395. doi:10.1016/0021-9797(87)90054-3.

[34] M. Vanni, Creeping flow over spherical permeable aggregates, Chemical Engineering Science 55 (2000) 685–698. doi:10.1016/S0009-2509(99)00316-4.

[35] B. O. Conchuir, Y. M. Harshe, M. Lattuada, A. Zaccone, Analytical model of fractal aggregate stability and restructuring in shear flows, Industrial & Engineering Chemistry Research 53 (2014) 9109–9119. doi:10.1021/ie4032605.

[36] J. G. M. Eggels, J. A. Somers, Numerical simulation of free convective flow using the lattice-Boltzmann scheme, International Journal of Heat and Fluid Flow 16 (1995) 357–364. doi:http://dx.doi.org/10.1016/0142-727X(95)00052-R.

[37] R. Sungkorn, J. J. Derksen, Simulations of dilute sedimenting suspensions at finite-particle reynolds numbers, Physics of Fluids 24 (2012) 123303.

[38] J. Gregory, The density of particle aggregates, Water Science and Technology 36 (1997) 1–13. doi:10.1016/S0273-1223(97)00452-6.

[39] L. Gmachowski, Calculation of the fractal dimension of aggregates, Colloids and Surfaces A: Physicochemical and Engineering Aspects 211 (2002) 197–203. doi:10.1016/S0927-7757(02)00278-9.

[40] Y. M. Harshe, L. Ehrl, M. Lattuada, Hydrodynamic properties of rigid fractal aggregates of arbitrary morphology, Journal of Colloid and Interface Science 352 (2010) 87–98. doi:10.1016/j.jcis.2010.08.040.

[41] T. Serra, X. Casamitjana, Structure of the aggregates during the process of aggregation and breakup under a shear flow, Journal of Colloid and Interface Science 206 (1998) 505–511. doi:10.1006/jcis.1998.5714.

[42] P. Jarvis, B. Jefferson, S. A. Parsons, Breakage, regrowth, and fractal nature of natural organic matter flocs, Environmental science & technology 39 (2005) 2307–2314. doi:10.1021/es048854x.

[43] A. S. Moussa, M. Soos, J. Sefcik, M. Morbidelli, Effect of solid volume fraction on aggregation and breakage in colloidal suspensions in batch and continuous stirred tanks, Langmuir 23 (2007) 1664–1673. doi:10.1021/la062138m.

[44] L. Guerin, C. Frances, A. Liné, C. Coufort-Saudejaud, Fractal dimensions and morphological characteristics of aggregates formed in different physico-chemical and mechanical flocculation environments, Colloids and Surfaces A: Physicochemical and Engineering Aspects 560 (2019) 213–222. doi:10.1016/j.colsurfa.2018.10.017.

[45] J. N. Israelachvili, Intermolecular and Surface Forces, Academic press, 2015.

[46] H. C. Hamaker, The London-van der Waals attraction between spherical particles, Physica 4 (1937) 1058–1072. doi:10.1016/S0031-8914(37)80203-7.

[47] D. L. Feke, N. D. Prabhu, J. A. J. Mann, J. A. L. Mann, A formulation of the short-range repulsion between spherical colloidal particles, The Journal of Physical Chemistry 88 (1984) 5735–5739. doi:10.1021/j150667a055.

[48] Y. M. Harshe, M. Lattuada, Universal breakup of colloidal clusters in simple shear flow, The Journal of Physical Chemistry B 120 (2016) 7244–7252. doi:10.1021/acs.jpcb.6b03220.

[49] M. Vanni, Accurate modelling of flow induced stresses in rigid colloidal aggregates, Computer Physics Communications 192 (2015) 70–90. doi:10.1016/j.cpc.2015.02.022.

[50] P. Adler, Streamlines in and around porous particles, Journal of Colloid and Interface Science 81 (1981) 531–535. doi:10.1016/0021-9797(81)90434-3.

[51] B. O. Conchúir, A. Zaccone, Mechanism of flow-induced biomolecular and colloidal aggregate breakup, Physical Review E 87 (2013) 032310. doi:10.1103/PhysRevE.87.032310.

[52] R. Di Felice, The voidage function for fluid-particle interaction systems, International Journal of Multiphase Flow 20 (1994) 153–159. doi:10.1016/0301-9322(94)90011-6.

[53] H. Haddadi, J. F. Morris, Topology of pair-sphere trajectories in finite inertia suspension shear flow and its effects on microstructure and rheology, Physics of Fluids 27 (2015) 043302. doi:10.1063/1.4917030.

[54] J.-S. Kroll-Rabotin, M. Gisselbrecht, B. Ott, R. May, J. Fröhlich, J.-P. Bellot, Multiscale simulation of non-metallic inclusion aggregation in a fully resolved bubble swarm in liquid steel, Metals 10 (2019) 517. doi:10.3390/met10040517.

Supporting Material

SM 1. Force Profile of Cohesive forces

The normal cohesive forces were described through a combination of van der Waals forces and Born repulsion. Since both of these forces linearly depend on the Hamaker constant, the maximum value of the net attractive force can be manipulated by varying the Hamaker constant. Fig. SM 1.1 shows the force profiles obtained for the values of Hamaker constant used in the manuscript. It can be seen that peak attraction is achieved at separation distance of less than 1 nm for the particles considered here, and this separation distance for maximum attractive force does not change with the Hamaker constant. Similarly, the equilibrium separation distance, that is the position of net zero force, is at 0.48 nm for all Hamaker constants. Although this equilibrium distance was used as the initial separation distance while generating aggregates, any other separation value also results in the particles to settle at this equilibrium condition by energy dissipation through viscous losses.

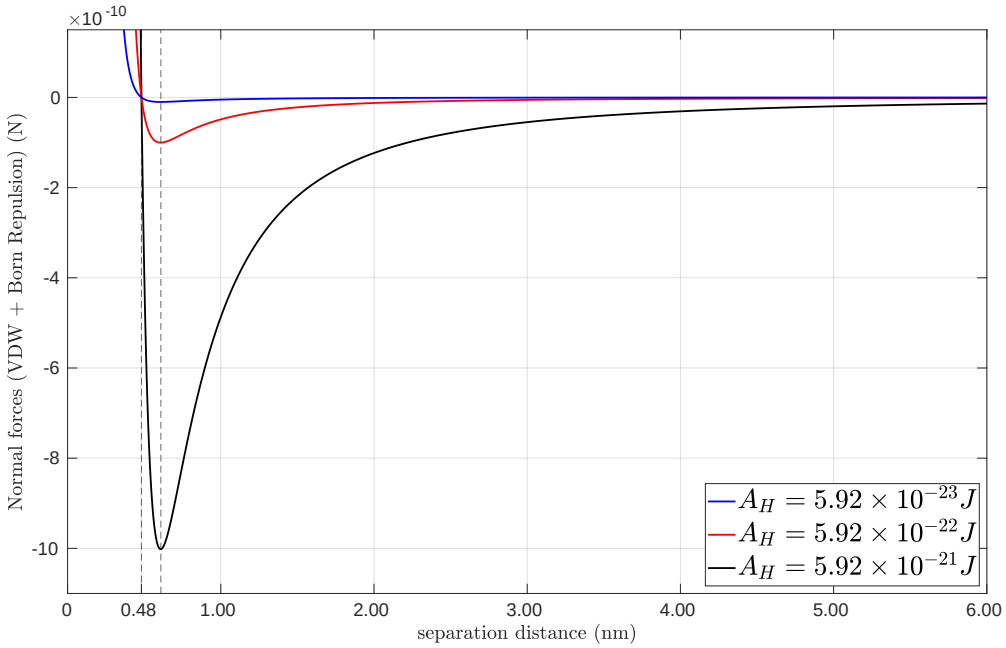

Figure SM 1.1: Normal force profile with separation distance for the considered values of Hamaker constant.

SM 2. Tangential Forces and associated critical elongation

The maximum tangential force F_t is defined as

$$F_t = k_t \, d_{\max} \tag{SM 1}$$

where k_t is spring stiffness and $d_{\max}$ is the maximum elongation allowed. The value of $d_{\max}$ was chosen considering two factors. First, it must be small compared to the particle size, preventing it from becoming another parameter which may influence the results. Secondly, too small value $d_{\max}$ can make the F_t over-sensitive to distance, resulting in force calculation to be numerically unstable. Therefore, a value of $d_{\max}$=0.02 R_p was chosen, and the maximum tangential force F_t was varied through k_t.

A tangential bond is formed between two particles when the surface-to-surface distance is shorter than $d_{\max}$. The tangential force increases with the elongation of the spring in the tangential direction until the maximum elongation $d_{\max}$ is reached. The spring then stops elongating any further and tangential forces remain capped to the corresponding maximum force. When the surface-to-surface distance exceeds $d_{\max}$, the tangential bond is broken, and no tangential force is applied anymore. If a new bond is made later between the same two particles, it starts with a spring elongation reset to 0.

SM 3. Equations in DEM

In DEM, particle velocities are calculated by solving Newton's equations of motion for every particle. The equations can be written as

$$m\frac{\mathrm{d}\boldsymbol{v}_i}{\mathrm{d}t} = \sum \boldsymbol{F}_i \tag{SM 2}$$

$$\mathcal{J}\frac{\mathrm{d}\boldsymbol{\omega}_i}{\mathrm{d}t} = \sum \boldsymbol{T}_i \tag{SM 3}$$

where $\boldsymbol{v}_i$ and $\boldsymbol{\omega}_i$ are velocity and angular velocity of particle i, and $\boldsymbol{F}_i$ and $\boldsymbol{T}_i$ are the forces and torques acting on the particle.

In this study, these equations are solved through a linear system of equations where all forces and torques that depend on particle acceleration and velocity are accounted for as linear functions. Forces are represented by coefficients α and β in:

$$m_p\frac{\mathrm{d}\boldsymbol{v}}{\mathrm{d}t} = \alpha\,\frac{\mathrm{d}\boldsymbol{v}}{\mathrm{d}t} + \beta\,\boldsymbol{v} + \boldsymbol{\gamma} \tag{SM 4}$$

The velocity calculation at each time step comes directly from Equation (SM 4) which yields a simple linear equation, i.e.

$$m_p\frac{\boldsymbol{v}(t) - \boldsymbol{v}(t-\Delta t)}{\Delta t} = \alpha\,\frac{\boldsymbol{v}(t) - \boldsymbol{v}(t-\Delta t)}{\Delta t} + \beta\,\boldsymbol{v}(t) + \boldsymbol{\gamma} \tag{SM 5}$$

Equation (SM 5) is solved for $\boldsymbol{v}(t)$ as

$$\boldsymbol{v}(t) = \frac{\left(\dfrac{m_p - \alpha}{\Delta t}\right)\boldsymbol{v}(t-\Delta t) + \boldsymbol{\gamma}}{\dfrac{m_p - \alpha}{\Delta t} - \beta} \tag{SM 6}$$

The term $\boldsymbol{\gamma}$ contains the forces that do not depend on particle motion, such as the particle-particle interactions. The term β contains velocity dependent terms. For example, in the simulations with FDA, the particle velocity term becomes $\beta = -6\pi\mu R_p$ and the fluid velocity term is expressed as $\boldsymbol{\gamma} = 6\pi\mu R_p\dot{\gamma}(z - z_C)$, where z is the cross-shear coordinate and z_C the center of the domain along that coordinate. In this study, particle intertia is negligible, which translates into Equation (SM 6) as $(m_p - \alpha)/\Delta t << \beta$ and $(m_p - \alpha)\boldsymbol{v}/\Delta t << \boldsymbol{\gamma}$ in FDA simulations.

Particle interactions through cohesive forces are implemented fully explicitly, in the $\boldsymbol{\gamma}$ term of Equation (SM 6). Since they are very short ranged, they impose very short time steps in the simulation to be captured accurately. Very short time steps are also required by low-Reynolds simulations with a LBM flow solver. In the end, because of the strong constraints limiting the time step, particle trajectory integration is achieved using a very simple Euler integration scheme as

$$\boldsymbol{x}(t + \Delta t) = \boldsymbol{x}(t) + \boldsymbol{v}(t)\,\Delta t \tag{SM 7}$$

SM 4. Evolution of all aggregates with modeled hydrodynamics (FDA)

The evolution of each aggregate under all considered force ratios is shown in Fig. SM 4.1. All graphs in the same column have the identical normal force ratio, while the tangential forces increase from top to bottom. It can be seen that aggregate to aggregate behavior for same force ratios can vary significantly (cases in point include $F_n^* = 10$ and $F_t^* \in \{.01, 0.1, 100\}$). Also, under the same conditions and force ratios, fate of the aggregates in terms of breakage or survival can be very different. Nonetheless, even in such a chaotic system, general trends can be observed: radii of gyration at the end of most simulation cases are distributed around an average value that clearly changes with force ratios. Meaningful data for restructuring can be extracted from aggregates that survive, while broken aggregates can provide information about breakage mechanism. Although some aggregates do not reach structural equilibrium in 6–7 rotations, all aggregates undergo enough restructuring to highlight the effects of the involved forces.

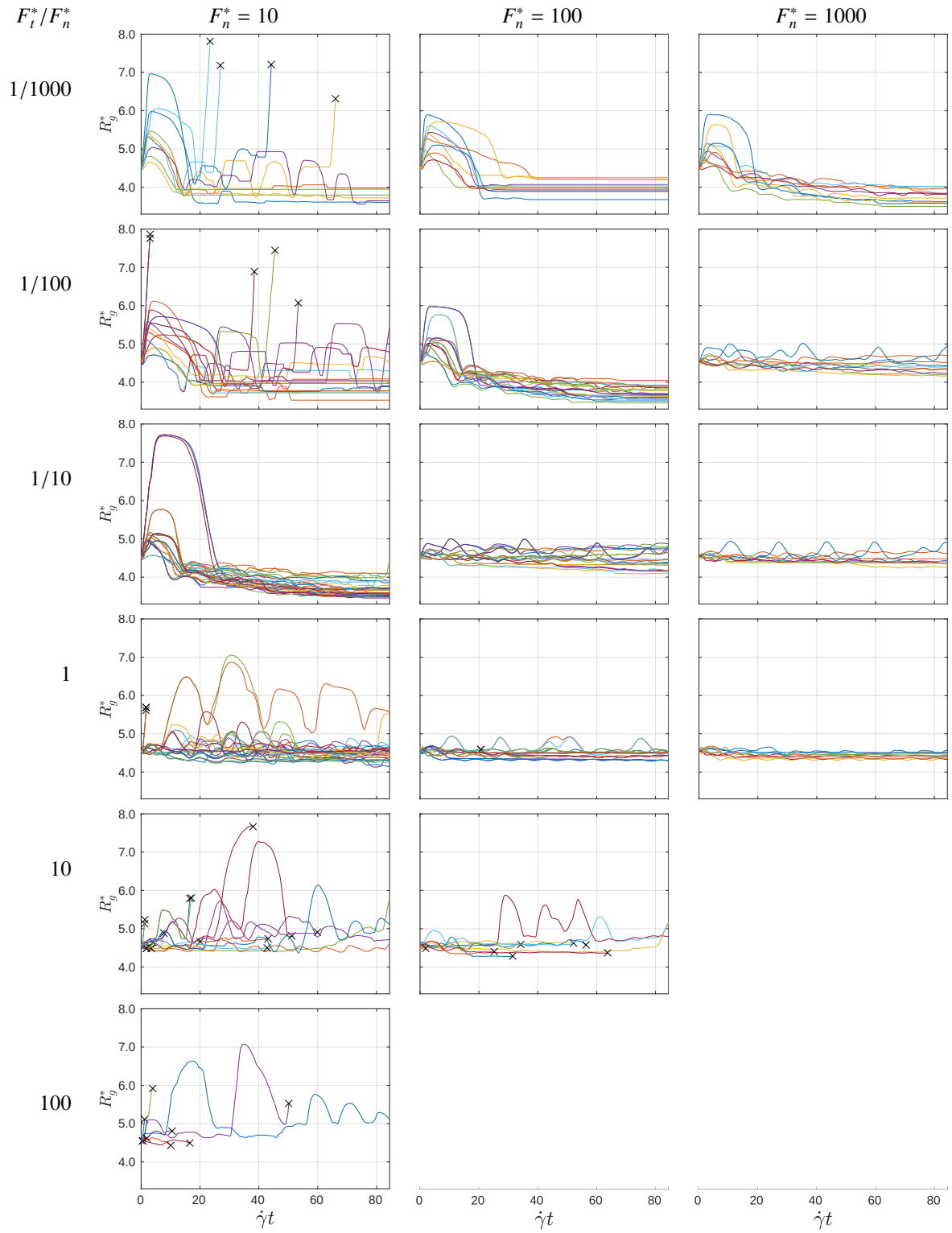

Figure SM 4.1: Evolution of aggregate size (R_g^*) for the force ratios considered in the present study. All breakage events are marked by '×'.

SM 5. Evolution of all aggregates with resolved hydrodynamics (LBM+IBM+DEM)

Time evolution of R_g^* for 4 different values of F_t^* are presented in Fig. SM 5.1. It can be seen that these results differ quite significantly from FDA results for similar conditions presented in the first column of Fig. SM 4.1. Aggregates do restructure, and show the same general trends as with FDA; that is, evolving towards denser structures over the duration of a simulation while going through significant elongations while rotating, particularly during their first cycles. However, their radii of gyration remain in a narrower range for all aggregates. This is especially noteworthy during the first rotation when the algorithmically created aggregates first adjust to the flow. In contrast, FDA shows much stronger restructuring for the first rotation. When the hydrodynamics are accurately resolved, less aggregate restructuring is observed, and the aggregates also break much less frequently. While small tangential forces lead to frequent breakage with FDA, such breakage does not occur with resolved hydrodynamics. These observations result from the combination of two phenomena induced by hydrodynamic interactions between particles in the aggregate: lubrication and decrease in strain rate.

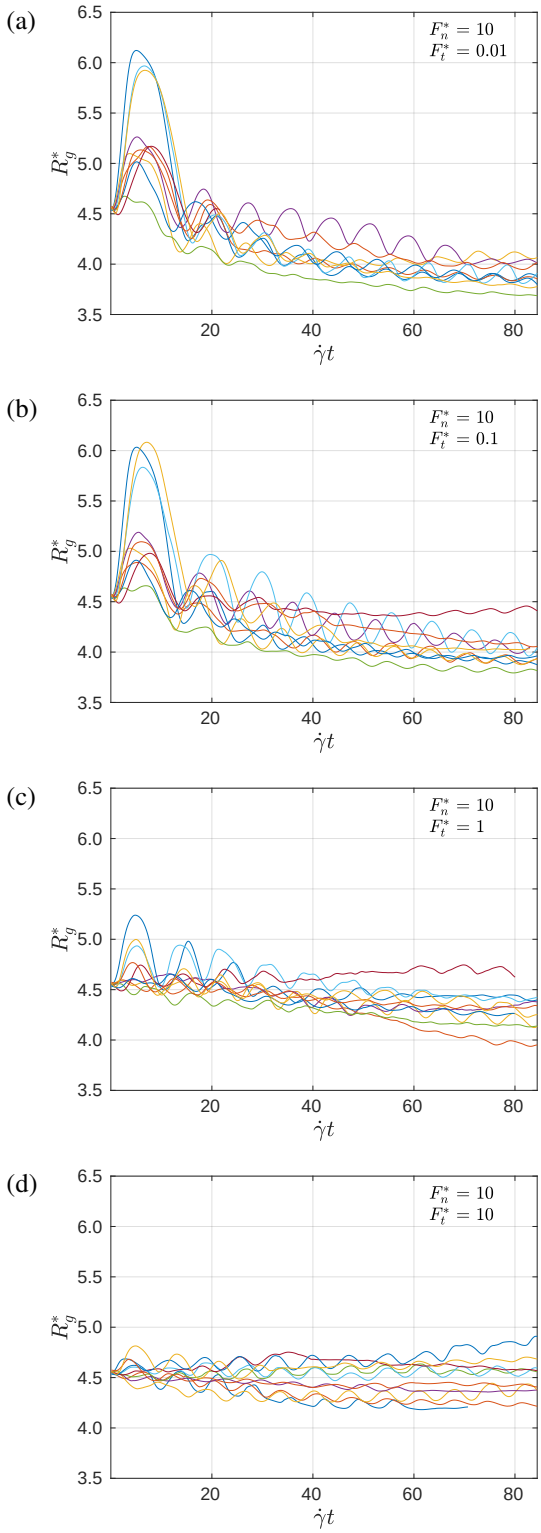

Figure SM 5.1: Size evolution of the 10 aggregates over a duration of 84.8 $\gamma\dot{t}$ with resolved hydrodynamics for force ratios $F_n^* = 10$ and (a) $F_t^* = 0.01$, (b) $F_t^* = 0.1$, (c) $F_t^* = 1$, and (d) $F_t^* = 10$.